

Muon-Pair and Tau-Pair Production in Two-Photon Collisions at LEP

L3 Collaboration

Abstract

The QED processes $e^+e^- \rightarrow e^+e^-\mu^+\mu^-$ and $e^+e^- \rightarrow e^+e^-\tau^+\tau^-$ are studied with the L3 detector at LEP using an untagged data sample collected at centre-of-mass energies $161 \text{ GeV} \leq \sqrt{s} \leq 209 \text{ GeV}$. The τ -pairs are observed through the associated decay of one τ into $e\nu\nu$ and the other into $\pi\pi\nu$. The cross sections are measured as a function of \sqrt{s} . For muon pairs, the cross section of the $\gamma\gamma \rightarrow \mu^+\mu^-$ process is also measured as a function of the two-photon centre-of-mass energy for $3 \text{ GeV} \leq W_{\gamma\gamma} \leq 40 \text{ GeV}$. Good agreement is found between these measurements and the $\mathcal{O}(\alpha^4)$ QED expectations. In addition, limits on the anomalous magnetic and electric dipole moments of the τ lepton are extracted.

Submitted to *Phys. Lett. B*

1 Introduction

The pair production of charged leptons in two-photon collisions offers a unique opportunity to test QED to $\mathcal{O}(\alpha^4)$ over a wide kinematical range. The $e^+e^- \rightarrow e^+e^-\mu^+\mu^-$ and $e^+e^- \rightarrow e^+e^-\tau^+\tau^-$ reactions are studied with the L3 detector [1] for untagged events, in which the e^+ and e^- , scattered at small angles, are not required to be observed.

Figure 1 shows the lowest order processes which contribute to this final state: multiperipheral, bremsstrahlung, annihilation and conversion, for a total of 12 possible diagrams. For untagged events the multiperipheral process dominates the cross section. The contribution of other processes is below 1%.

The $e^+e^- \rightarrow e^+e^-\ell^+\ell^-$ reactions, where $\ell = e, \mu$ or τ , were previously studied for untagged two-photon events at e^+e^- centre-of-mass energy, \sqrt{s} , close to the Z mass [2]. Good agreement was found between the measurements and the QED expectations. In this Letter, the production of μ -pairs is studied in the range $161 \text{ GeV} \leq \sqrt{s} \leq 209 \text{ GeV}$ and the production of τ -pairs in the range $189 \text{ GeV} \leq \sqrt{s} \leq 209 \text{ GeV}$. The individual energies and luminosities are listed in Table 1. As the $e^+e^- \rightarrow e^+e^-\mu^+\mu^-$ channel benefits from high statistics, the cross section of the process $\gamma\gamma \rightarrow \mu^+\mu^-$ is also measured as a function of the two-photon centre-of-mass energy, $W_{\gamma\gamma}$. The $e^+e^- \rightarrow e^+e^-\tau^+\tau^-$ analysis is restricted to the exclusive final state where $\tau^- \rightarrow e^-\nu_\tau\bar{\nu}_e$ and $\tau^+ \rightarrow \pi^+\pi^0\nu_\tau^1$, which arises from $9.07 \pm 0.01\%$ of all τ -pair decays [3].

The process $e^+e^- \rightarrow e^+e^-\tau^+\tau^-$ is also used to constrain the anomalous magnetic and electric dipole moments of the τ lepton, as proposed in Reference 4.

2 Data and Monte Carlo Samples

The events are mainly accepted by the charged-particle [6] and the inner track triggers [5]. The former requires at least two charged particles with a transverse momentum $p_t > 150 \text{ MeV}$, back-to-back within an acoplanarity angle of $\pm 41^\circ$. The latter is based on a neural network, has no requirement on the acoplanarity angle of the tracks and extends the acceptance from the polar region $30^\circ < \theta < 150^\circ$ to $15^\circ < \theta < 165^\circ$. A fraction of the $e^+e^- \rightarrow e^+e^-\mu^+\mu^-$ events is also accepted by the muon trigger and a fraction of the $e^+e^- \rightarrow e^+e^-\tau^+\tau^-$ events by the calorimetric energy trigger [7].

The DIAG36 [8] generator is used to calculate at $\mathcal{O}(\alpha^4)$ the full set of diagrams shown in Figure 1. To obtain the efficiencies of the $e^+e^- \rightarrow e^+e^-\mu^+\mu^-$ channel, high statistics samples are generated in the range $3 \text{ GeV} \leq W_{\gamma\gamma} \leq 40 \text{ GeV}$, for each value of \sqrt{s} . The $e^+e^- \rightarrow e^+e^-\tau^+\tau^-$ events are generated in the full phase space with the Vermaseren Monte Carlo [9], which takes into account only the dominating multiperipheral diagrams, shown in Figure 1a.

For background studies, the following event generators are used: KORALZ [10] for the $e^+e^- \rightarrow \tau^+\tau^-$ and $e^+e^- \rightarrow \mu^+\mu^-$ processes and LEPWW [11] and PYTHIA [12] for W and Z boson pair-production and decays into leptons, respectively. In the tau-pair analysis, exclusive hadronic two-photon processes are generated with EGPC [13] and inclusive hadron production with PHOJET [14].

All generated events are processed through the full L3 detector simulation based on the GEANT [15] and GHEISHA [16] programs and are reconstructed following the same procedure as for the data. Time dependent detector inefficiencies, as monitored during the data taking, are also included.

¹)Charge conjugate processes are included throughout this Letter.

3 Event Selection

3.1 $e^+e^- \rightarrow e^+e^-\mu^+\mu^-$

The muon pairs are selected using information from the central tracking chamber (TEC) and the muon spectrometer. The selection requires:

- exactly two tracks with at least 12 hits each and opposite charges, having a distance of closest approach to the nominal interaction vertex in the plane transverse to the beam direction smaller than 5 mm;
- two well reconstructed muons in the muon chambers corresponding to the charged tracks;
- a fiducial volume $|\cos\theta_\mu| < 0.8$, where θ_μ is the angle between the muon and the beam axis;
- the momentum of the muons between 2.5 GeV and 40 GeV;
- muon tracks pointing to the primary vertex, with time-of-flight consistent with the beam crossing, in order to suppress background from cosmic rays, hadrons decaying in flight and punch-through hadrons;
- a di-muon effective mass, $M_{\mu\mu}$, which measures $W_{\gamma\gamma}$, between 3 GeV and 40 GeV.

The numbers of events selected at different \sqrt{s} are shown in Table 1 together with the selection and trigger efficiencies. The total background contribution, estimated by Monte Carlo, is below 1%, and consists mainly of events from the $e^+e^- \rightarrow e^+e^-\tau^+\tau^-$, $e^+e^- \rightarrow \tau^+\tau^-$ and $e^+e^- \rightarrow \mu^+\mu^-$ processes and cosmic rays. The distributions of the di-muon effective mass and of the momentum of the higher energy muon are presented in Figure 2a and 2b together with the Monte Carlo predictions. The expected distributions agree well with the data.

3.2 $e^+e^- \rightarrow e^+e^-\tau^+\tau^-$

The selection of tau-pairs, through the associated decays $\tau^- \rightarrow e^-\nu_\tau\bar{\nu}_e$ and $\tau^+ \rightarrow \pi^+\pi^0\bar{\nu}_\tau$, is based on information from the TEC and the electromagnetic calorimeter (ECAL). It requires:

- a total energy in the calorimeters less than 40 GeV, to exclude $e^+e^- \rightarrow \tau^+\tau^-$ events;
- exactly two charged tracks with at least 12 hits each and opposite charges, having a transverse momentum greater than 0.3 GeV, a distance of closest approach to the nominal interaction vertex in the plane transverse to the beam direction smaller than 10 mm and a corresponding ECAL signal;
- two photons, defined as isolated showers in the ECAL with energy greater than 100 MeV distributed over at least two crystals. There must be no track within 150 mrad around the shower direction and the ratio between the energies deposited in the hadronic and electromagnetic calorimeters must be less than 0.2.

The electron identification for the reaction $\tau^- \rightarrow e^- \nu_\tau \bar{\nu}_e$ is based on an ECAL cluster, with a shower shape consistent with that of an electromagnetic particle, matching with a charged track within 100 mrad in the plane transverse to the beam direction. The momentum of the electron candidate must be greater than 600 MeV. To achieve high efficiency and high purity, the electron identification is based on a neural network [17] which combines ten variables: the energy in ECAL, the momentum, the ionisation energy loss in TEC, the ratio of the transverse energy in ECAL to the transverse momentum in TEC, the number of crystals in the shower, three inputs describing the shower shape in ECAL, the corresponding energy in the hadronic calorimeter and its fraction within a 7° cone. The electron identification with the neural network has an efficiency of $87.7 \pm 0.2\%$ with a purity of $94.7 \pm 0.2\%$, as determined from Monte Carlo events.

To identify $\tau^+ \rightarrow \pi^+ \pi^0 \bar{\nu}_\tau$ decays, we require the two photons to be compatible with a π^0 . The remaining charged particle is considered to be the π^+ candidate. No additional selection cut is applied on the π^+ . The two-photon effective mass distribution in Figure 3a shows the π^0 peak. A gaussian fit to this peak gives a mass of 134.6 ± 0.6 MeV and a width of 6.8 ± 0.7 MeV, compatible with the expected detector resolution. We require the two-photon effective mass to be within the range from 115 MeV to 155 MeV. To reject exclusive final states, as for example $e^+e^- \rightarrow e^+e^- a_2(1320) \rightarrow e^+e^- \pi^+ \pi^- \pi^0$, we require the total transverse momentum imbalance $|\sum \vec{p}_t|$ to be greater than 0.2 GeV. Figure 3b compares the $|\sum \vec{p}_t|$ distribution of data and Monte Carlo. The excess of data for $|\sum \vec{p}_t| < 0.2$ GeV is due to exclusive two-photon processes not included in the Monte Carlo.

With these criteria, 266 events are selected. As expected for the $\tau^+ \rightarrow \pi^+ \pi^0 \bar{\nu}_\tau$ decay channel, the $\pi^+ \pi^0$ effective mass is consistent with the ρ meson mass, as shown in Figure 3c. The energy distribution of the electron candidate is shown in Figure 3d. All data distributions are in good agreement with Monte Carlo simulations.

Table 1 shows the number of observed events together with selection and trigger efficiencies. The latter are evaluated directly from the data [18]. In the analysis, a two dimensional trigger efficiency correction, based on the highest momentum track and the azimuthal opening angle between the two tracks, is applied to each event. The main background in the sample is 26% and is due to tau-pairs decaying to other final states, where leptons or pions are misidentified, or additional pions are not detected. The background from the $e^+e^- \rightarrow \tau^+ \tau^-$ process, from resonant final states and from hadron production in two-photon collisions is less than 4%. The background from beam-gas and beam-wall interactions is found to be negligible.

4 Results

4.1 $e^+e^- \rightarrow e^+e^- \mu^+ \mu^-$

The cross-section of the process $e^+e^- \rightarrow e^+e^- \mu^+ \mu^-$ for $3 \text{ GeV} < W_{\gamma\gamma} < 40 \text{ GeV}$ is measured for $|\cos \theta_\mu| < 0.8$ and extrapolated to the full angular range. The results are given in Table 2 for different values of \sqrt{s} .

For lower luminosities the systematic uncertainties are dominated by the uncertainty on the trigger efficiency, around 3%. At higher luminosities the main uncertainty of about 1.5% arises from the limited Monte Carlo statistics. The uncertainty due to the event selection is estimated by varying the selection criteria for the data samples with high integrated luminosity and is less than 1%.

The cross section for the full angular range, presented in Figure 4, shows the expected slow

rise as a function of \sqrt{s} and is in good agreement with the QED prediction, as calculated by DIAG36 Monte Carlo. The cross section of the process $\gamma\gamma \rightarrow \mu^+\mu^-$ is derived by measuring the cross section of the $e^+e^- \rightarrow e^+e^-\mu^+\mu^-$ process in nine $W_{\gamma\gamma}$ bins and scaling it by the two-photon luminosity function [19]. The values obtained at different \sqrt{s} are consistent within a given $W_{\gamma\gamma}$ bin, as shown in Table 3 and Figure 5a. Combined results for the full data sample are listed in Table 3 and shown in Figure 5b together with the QED predictions. A good agreement is observed.

4.2 $e^+e^- \rightarrow e^+e^-\tau^+\tau^-$

The total τ -pair production cross section is given in Table 2. The cross section is lower than the $e^+e^- \rightarrow e^+e^-\mu^+\mu^-$ cross section because of the τ -pair mass threshold of 3.6 GeV. The main contributions to systematic uncertainties comes from the variation of the cuts on $|\sum \vec{p}_t|$ and the electron momentum, both between 4% and 5%. The total systematic uncertainty due to selection criteria is estimated to be between 7% and 9%. Other sources of systematic uncertainties are the determination of the trigger efficiency, the Monte Carlo statistics and the uncertainty on the background level; their combined contribution is below 3%. Figure 4 compares the measured cross section and the $\mathcal{O}(\alpha^4)$ QED calculation. A good agreement is found.

4.3 Anomalous Couplings of the Tau Lepton

Photon couplings to the tau lepton are in general due to its electric charge, the magnetic dipole moment and the electric dipole moment. They can be described by a matrix element in which the usual γ^μ term is replaced by [20]:

$$\Gamma^\mu = F_1(q^2)\gamma^\mu + iF_2(q^2)\sigma^{\mu\nu}\frac{q_\nu}{2m_\tau} + F_3(q^2)\gamma_5\sigma^{\mu\nu}\frac{q_\nu}{2m_\tau},$$

where the form factors $F_1(q^2)$, $F_2(q^2)$ and $F_3(q^2)$, functions of the four-momentum squared, q^2 , of the photon, are related to the tau charge, magnetic and electric dipole moments as:

$$e_\tau = eF_1(0), \quad \mu_\tau = \frac{e(F_1(0) + F_2(0))}{2m_\tau}, \quad d_\tau = -\frac{eF_3(0)}{2m_\tau},$$

respectively. In the Standard Model, at tree level, $F_1(q^2) = 1$ and $F_2(q^2) = F_3(q^2) = 0$. Limits on $F_2(q^2)$ and $F_3(q^2)$ were derived from the decay width $\Gamma(Z \rightarrow \tau^+\tau^-)$, relating the $Z\tau\tau$ coupling to the photon couplings via $SU(2) \times U(1)$ invariance [21]. Direct studies of the $\gamma\tau\tau$ couplings were performed at the Z pole, by the L3 [22] and OPAL [23] collaborations through the $e^+e^- \rightarrow Z \rightarrow \tau^+\tau^-\gamma$ process, and at the $\Upsilon(4S)$ by the BELLE collaboration through the $e^+e^- \rightarrow \gamma^* \rightarrow \tau^+\tau^-$ process [24].

Tau-pair production in two-photon collisions is sensitive to possible anomalous couplings of the tau lepton. Values of $F_2(q^2)$ and d_τ different from zero would modify the cross section of the $e^+e^- \rightarrow e^+e^-\tau^+\tau^-$ process [4]. By comparing the measured cross section with predictions [4] as a function of $F_2(q^2)$ and d_τ we obtain:

$$|F_2(0)| \leq 0.107, \quad |d_\tau| \leq 1.14 \cdot 10^{-15} \text{ e cm}$$

at 95% confidence level, where the limit on each coupling is derived fixing the other coupling to zero. These bounds, limited by the size of the data sample, are in agreement with the more stringent published ones [22–24] and are derived from a different process.

References

- [1] L3 Collab., B. Adeva *et al.*, Nucl. Instr. Meth. **A 289** (1990) 35;
L3 Collab., O. Adriani *et al.*, Phys. Rep. **236** (1993) 1;
J.A. Bakken *et al.*, Nucl. Instr. Meth. **A 275** (1989) 81;
O. Adriani *et al.*, Nucl. Instr. Meth. **A 302** (1991) 53;
B. Adeva *et al.*, Nucl. Instr. Meth. **A 323** (1992) 109;
K. Deiters *et al.*, Nucl. Instr. Meth. **A 323** (1992) 162;
M. Chemarin *et al.*, Nucl. Instr. Meth. **A 349** (1994) 345;
M. Acciarri *et al.*, Nucl. Instr. Meth. **A 351** (1994) 300;
G. Basti *et al.*, Nucl. Instr. Meth. **A 374** (1996) 293;
A. Adam *et al.*, Nucl. Instr. Meth. **A 383** (1996) 342.
- [2] L3 Collab., M. Acciarri *et al.*, Phys. Lett. **B 407** (1997) 341.
OPAL Collab., R. Akers *et al.*, Z. Phys. C **60** (1993) 593.
- [3] K. Hagiwara *et al.*, Phys. Rev. **D 66** (2002) 010001.
- [4] F. Cornet and J.I. Illana, Phys. Rev. **D 53** (1996) 1181.
We wish to thank the authors for helpful discussions.
- [5] D. Haas *et al.*, Nucl. Instr. Meth. **A 420** (1999) 101.
- [6] P. Béné *et al.*, Nucl. Instr. Meth. **A 306** (1991) 150.
- [7] R. Bizzarri *et al.*, Nucl. Instr. Meth. **A 283** (1989) 799.
- [8] DIAG36 Monte Carlo;
F.A. Berends, P.H. Daverveldt and R. Kleiss., Nucl. Phys. **B 253** (1985) 441.
- [9] J.A.M. Vermaseren, Nucl. Phys. **B 229** (1983) 347.
- [10] KORALZ version 4.02 is used;
S. Jadach, B.F.L. Ward and Z. Wąs, Comp. Phys. Comm. **79** (1994) 503.
- [11] LEPWW Monte Carlo;
F.C. Erné, *Physics at LEP2*, eds. G. Altarelli, T. Sjöstrand and F. Zwirner, CERN 96-01 (1996), vol.2 pag.36.
- [12] PYTHIA version 5.772 is used;
T. Sjöstrand, Comp. Phys. Comm. **82** (1994) 74.
- [13] EGPC Monte Carlo;
F. Linde, *Workshop on detector and event simulation in high energy physics Monte Carlo*, eds. K. Bos and B. van Eijl, Amsterdam (1991).
- [14] PHOJET version 1.05c is used;
R. Engel, Z. Phys. **C 66** (1995) 203;
R. Engel and J. Ranft, Phys. Rev. **D 54** (1996) 4244.
- [15] GEANT version 3.15 is used;
R. Brun *et al.*, preprint CERN-DD/EE/84-1 (1984), revised 1987.

- [16] H. Fesefeldt, RWTH Aachen report PITHA 85/2 (1985).
- [17] Stuttgart Neural Network Simulator, <http://www-ra.informatik.uni-tuebingen.de/SNNS/>.
- [18] D. Haas, PhD Thesis, University of Basel (2000).
- [19] G.A. Schuler, preprint hep-ph/9610406 (1996).
- [20] C. Itzykson and J.B. Zuber, *Quantum Field Theory*, McGraw-Hill, New York (1980).
- [21] R. Escribano and E. Masso, Phys. Lett. **B 395** (1997) 369.
- [22] L3 Collab., M. Acciarri *et al.*, Phys. Lett. **B 434** (1998) 169.
- [23] OPAL Collab., K. Ackerstaff *et al.*, Phys. Lett. **B 431** (1998) 188.
- [24] BELLE Collab., K. Inami *et al.*, Phys. Lett. **B 551** (2003) 16.

The L3 Collaboration:

P.Achard,²⁰ O.Adriani,¹⁷ M.Aguilar-Benitez,²⁴ J.Alcaraz,²⁴ G.Alemanni,²² J.Allaby,¹⁸ A.Aloisio,²⁸ M.G.Alvigi,²⁸ H.Anderhub,⁴⁶ V.P.Andreev,^{6,33} F.Anselmo,⁸ A.Arefiev,²⁷ T.Azemoon,³ T.Aziz,⁹ P.Bagnaia,³⁸ A.Bajo,²⁴ G.Baksay,²⁵ L.Baksay,²⁵ S.V.Baldew,² S.Banerjee,⁹ Sw.Banerjee,⁴ A.Barczyk,^{46,44} R.Barillère,¹⁸ P.Bartalini,²² M.Basile,⁸ N.Batalova,⁴³ R.Battiston,³² A.Bay,²² F.Becattini,¹⁷ U.Becker,¹³ F.Behner,⁴⁶ L.Bellucci,¹⁷ R.Berbeco,³ J.Berdugo,²⁴ P.Berges,¹³ B.Bertucci,³² B.L.Betev,⁴⁶ M.Biasini,³² M.Biglietti,²⁸ A.Biland,⁴⁶ J.J.Blaising,⁴ S.C.Blyth,³⁴ G.J.Bobbink,² A.Böhm,¹ L.Boldizar,¹² B.Borgia,³⁸ S.Bottai,¹⁷ D.Bourilkov,⁴⁶ M.Bourquin,²⁰ S.Braccini,²⁰ J.G.Branson,⁴⁰ F.Brochu,⁴ J.D.Burger,¹³ W.J.Burger,³² X.D.Cai,¹³ M.Capell,¹³ G.Cara Romeo,⁸ G.Carlino,²⁸ A.Cartacci,¹⁷ J.Casaus,²⁴ F.Cavallari,³⁸ N.Cavallo,³⁵ C.Cecchi,³² M.Cerrada,²⁴ M.Chamizo,²⁰ Y.H.Chang,⁴⁸ M.Chemarin,²³ A.Chen,⁴⁸ G.Chen,⁷ G.M.Chen,⁷ H.F.Chen,²¹ H.S.Chen,⁷ G.Chiefari,²⁸ L.Cifarelli,³⁹ F.Cindolo,⁸ I.Clare,¹³ R.Clare,³⁷ G.Coignet,⁴ N.Colino,²⁴ S.Costantini,³⁸ B.de la Cruz,²⁴ S.Cucciarelli,³² J.A.van Dalen,³⁰ R.de Asmundis,²⁸ P.Déglon,²⁰ J.Debreczeni,¹² A.Degré,⁴ K.Dehmelt,²⁵ K.Deiters,⁴⁴ D.della Volpe,²⁸ E.Delmeire,²⁰ P.Denes,³⁶ F.DeNotaristefani,³⁸ A.De Salvo,⁴⁶ M.Diemoz,³⁸ M.Dierckxsens,² C.Dionisi,³⁸ M.Dittmar,⁴⁶ A.Doria,²⁸ M.T.Dova,^{10,†} D.Duchesneau,⁴ M.Duda,¹ B.Echenard,²⁰ A.Eline,¹⁸ A.El Hage,¹ H.El Mamouni,²³ A.Engler,³⁴ F.J.Eppling,¹³ P.Extermann,²⁰ M.A.Falagan,²⁴ S.Falciano,³⁸ A.Favara,³¹ J.Fay,²³ O.Fedin,³³ M.Felcini,⁴⁶ T.Ferguson,³⁴ H.Fesefeldt,¹ E.Fiandrini,³² J.H.Field,²⁰ F.Filthaut,³⁰ P.H.Fisher,¹³ W.Fisher,³⁶ I.Fisk,⁴⁰ G.Forconi,¹³ K.Freundreich,⁴⁶ C.Furetta,²⁶ Yu.Galaktionov,^{27,13} S.N.Ganguli,⁹ P.Garcia-Abia,²⁴ M.Gataullin,³¹ S.Gentile,³⁸ S.Giagu,³⁸ Z.F.Gong,²¹ G.Grenier,²³ O.Grimm,⁴⁶ M.W.Gruenewald,¹⁶ M.Guida,³⁹ R.van Gulik,² V.K.Gupta,³⁶ A.Gurtu,⁹ L.J.Gutay,⁴³ D.Haas,⁵ D.Hatzifotiadou,⁸ T.Hebbeker,¹ A.Hervé,¹⁸ J.Hirschfelder,³⁴ H.Hofer,⁴⁶ M.Hohlmann,²⁵ G.Holzner,⁴⁶ S.R.Hou,⁴⁸ Y.Hu,³⁰ B.N.Jin,⁷ L.W.Jones,³ P.de Jong,² I.Josa-Mutuberría,²⁴ M.Kaur,¹⁴ M.N.Kienzle-Focacci,²⁰ J.K.Kim,⁴² J.Kirkby,¹⁸ W.Kittel,³⁰ A.Klimentov,^{13,27} A.C.König,³⁰ M.Kopal,⁴³ V.Koutsenko,^{13,27} M.Kräber,⁴⁶ R.W.Kraemer,³⁴ A.Krüger,⁴⁵ A.Kunin,¹³ P.Ladron de Guevara,²⁴ I.Laktineh,²³ G.Landi,¹⁷ M.Lebeau,¹⁸ A.Lebedev,¹³ P.Lebrun,²³ P.Lecomte,⁴⁶ P.Lecoq,¹⁸ P.Le Coultre,⁴⁶ J.M.Le Goff,¹⁸ R.Leiste,⁴⁵ M.Levtchenko,²⁶ P.Levtchenko,³³ C.Li,²¹ S.Likhoded,⁴⁵ C.H.Lin,⁴⁸ W.T.Lin,⁴⁸ F.L.Linde,²⁸ L.Lista,²⁸ Z.A.Liu,⁷ W.Lohmann,⁴⁵ E.Longo,³⁸ Y.S.Lu,⁷ C.Luci,³⁸ L.Luminari,³⁸ W.Lustermann,⁴⁶ W.G.Ma,²¹ L.Malgeri,²⁰ A.Malinin,²⁷ C.Maña,²⁴ J.Mans,³⁶ J.P.Martin,²³ F.Marzano,³⁸ K.Mazumdar,⁹ R.R.McNeil,¹⁶ S.Mele,^{18,28} L.Merola,²⁸ M.Meschini,¹⁷ W.J.Metzger,³⁰ A.Mihul,¹¹ H.Milcent,¹⁸ G.Mirabelli,³⁸ J.Mnich,¹ G.B.Mohanty,⁹ G.S.Muanza,²³ A.J.M.Muijs,² B.Musicar,⁴⁰ M.Musy,³⁸ S.Nagy,¹⁵ S.Natale,²⁰ M.Napolitano,²⁸ F.Nessi-Tedaldi,⁴⁶ H.Newman,³¹ A.Nisati,³⁸ T.Novak,³⁰ H.Nowak,⁴⁵ R.Ofierzynski,⁴⁶ G.Organtini,³⁸ I.Pal,⁴³ C.Palomares,²⁴ P.Paolucci,²⁸ R.Paramatti,³⁸ G.Passaleva,¹⁷ S.Patricelli,²⁸ T.Paul,¹⁰ M.Pauluzzi,³² C.Paus,¹³ F.Pauss,⁴⁶ M.Pedace,³⁸ S.Pensotti,²⁶ D.Perret-Gallix,⁴ B.Petersen,³⁰ D.Piccolo,²⁸ F.Pierella,⁸ M.Pioppi,³² P.A.Piroué,³⁶ E.Pistoiesi,²⁶ V.Plyaskin,²⁷ M.Pohl,²⁰ V.Pojidaev,¹⁷ J.Pothier,¹⁸ D.Prokofiev,³³ J.Quartieri,³⁹ G.Rahal-Callot,⁴⁶ M.A.Rahaman,⁹ P.Raics,¹⁵ N.Raja,⁹ R.Ramelli,⁴⁶ P.G.Rancoita,²⁶ R.Ranieri,¹⁷ A.Raspereza,⁴⁵ P.Razis,²⁹ D.Ren,⁴⁶ M.Rescigno,³⁸ S.Reucroft,¹⁰ S.Riemann,⁴⁵ K.Riles,³ B.P.Roe,³ L.Romero,²⁴ A.Rosca,⁴⁵ C.Rosemann,¹ C.Rosenbleck,¹ S.Rosier-Lees,⁴ S.Roth,¹ J.A.Rubio,¹⁸ G.Ruggiero,¹⁷ H.Rykaczewski,⁴⁶ A.Sakharov,⁴⁶ S.Saremi,⁶ S.Sarkar,³⁸ J.Salicio,¹⁸ E.Sanchez,²⁴ C.Schäfer,¹⁸ V.Schegelsky,³³ H.Schopper,⁴⁷ D.J.Schotanus,³⁰ C.Sciacca,²⁸ L.Servoli,³² S.Shevchenko,³¹ N.Shivarov,⁴¹ V.Shoutko,¹³ E.Shumilov,²⁷ A.Shvorob,³¹ D.Son,⁴² C.Souga,²³ P.Spillantini,¹⁷ M.Steuer,¹³ D.P.Stickland,³⁶ B.Stoyanov,⁴¹ A.Straessner,²⁰ K.Sudhakar,⁹ G.Sultanov,⁴¹ L.Z.Sun,²¹ S.Sushkov,¹ H.Suter,⁴⁶ J.D.Swain,¹⁰ Z.Szillasi,^{25,¶} X.W.Tang,⁷ P.Tarjan,¹⁵ L.Tauscher,⁵ L.Taylor,¹⁰ B.Tellili,²³ D.Teyssier,²³ C.Timmermans,³⁰ Samuel C.C.Ting,¹³ S.M.Ting,¹³ S.C.Tonwar,⁹ J.Tóth,¹² C.Tully,³⁶ K.L.Tung,⁷ J.Ulbricht,⁴⁶ E.Valente,³⁸ R.T.Van de Walle,³⁰ R.Vasquez,⁴³ V.Veszpremi,²⁵ G.Vesztergombi,¹² I.Vetlitsky,²⁷ D.Vicinanza,³⁹ G.Viertel,⁴⁶ S.Villa,³⁷ M.Vivargent,⁴ S.Vlachos,⁵ I.Vodopianov,²⁵ H.Vogel,³⁴ H.Vogt,⁴⁵ I.Vorobiev,^{34,27} A.A.Vorobyov,³³ M.Wadhwa,⁵ Q.Wang,³⁰ X.L.Wang,²¹ Z.M.Wang,²¹ M.Weber,¹⁸ H.Wilkins,³⁰ S.Wynhoff,³⁶ L.Xia,³¹ Z.Z.Xu,²¹ J.Yamamoto,³ B.Z.Yang,²¹ C.G.Yang,⁷ H.J.Yang,³ M.Yang,⁷ S.C.Yeh,⁴⁹ An.Zalite,³³ Yu.Zalite,³³ Z.P.Zhang,²¹ J.Zhao,²¹ G.Y.Zhu,⁷ R.Y.Zhu,³¹ H.L.Zhuang,⁷ A.Zichichi,^{8,18,19} B.Zimmermann,⁴⁶ M.Zöller,¹

- 1 III. Physikalisches Institut, RWTH, D-52056 Aachen, Germany[§]
 - 2 National Institute for High Energy Physics, NIKHEF, and University of Amsterdam, NL-1009 DB Amsterdam, The Netherlands
 - 3 University of Michigan, Ann Arbor, MI 48109, USA
 - 4 Laboratoire d'Annecy-le-Vieux de Physique des Particules, LAPP,IN2P3-CNRS, BP 110, F-74941 Annecy-le-Vieux CEDEX, France
 - 5 Institute of Physics, University of Basel, CH-4056 Basel, Switzerland
 - 6 Louisiana State University, Baton Rouge, LA 70803, USA
 - 7 Institute of High Energy Physics, IHEP, 100039 Beijing, China[△]
 - 8 University of Bologna and INFN-Sezione di Bologna, I-40126 Bologna, Italy
 - 9 Tata Institute of Fundamental Research, Mumbai (Bombay) 400 005, India
 - 10 Northeastern University, Boston, MA 02115, USA
 - 11 Institute of Atomic Physics and University of Bucharest, R-76900 Bucharest, Romania
 - 12 Central Research Institute for Physics of the Hungarian Academy of Sciences, H-1525 Budapest 114, Hungary[‡]
 - 13 Massachusetts Institute of Technology, Cambridge, MA 02139, USA
 - 14 Panjab University, Chandigarh 160 014, India.
 - 15 KLTE-ATOMKI, H-4010 Debrecen, Hungary[¶]
 - 16 Department of Experimental Physics, University College Dublin, Belfield, Dublin 4, Ireland
 - 17 INFN Sezione di Firenze and University of Florence, I-50125 Florence, Italy
 - 18 European Laboratory for Particle Physics, CERN, CH-1211 Geneva 23, Switzerland
 - 19 World Laboratory, FBLJA Project, CH-1211 Geneva 23, Switzerland
 - 20 University of Geneva, CH-1211 Geneva 4, Switzerland
 - 21 Chinese University of Science and Technology, USTC, Hefei, Anhui 230 029, China[△]
 - 22 University of Lausanne, CH-1015 Lausanne, Switzerland
 - 23 Institut de Physique Nucléaire de Lyon, IN2P3-CNRS, Université Claude Bernard, F-69622 Villeurbanne, France
 - 24 Centro de Investigaciones Energéticas, Medioambientales y Tecnológicas, CIEMAT, E-28040 Madrid, Spain^b
 - 25 Florida Institute of Technology, Melbourne, FL 32901, USA
 - 26 INFN-Sezione di Milano, I-20133 Milan, Italy
 - 27 Institute of Theoretical and Experimental Physics, ITEP, Moscow, Russia
 - 28 INFN-Sezione di Napoli and University of Naples, I-80125 Naples, Italy
 - 29 Department of Physics, University of Cyprus, Nicosia, Cyprus
 - 30 University of Nijmegen and NIKHEF, NL-6525 ED Nijmegen, The Netherlands
 - 31 California Institute of Technology, Pasadena, CA 91125, USA
 - 32 INFN-Sezione di Perugia and Università Degli Studi di Perugia, I-06100 Perugia, Italy
 - 33 Nuclear Physics Institute, St. Petersburg, Russia
 - 34 Carnegie Mellon University, Pittsburgh, PA 15213, USA
 - 35 INFN-Sezione di Napoli and University of Potenza, I-85100 Potenza, Italy
 - 36 Princeton University, Princeton, NJ 08544, USA
 - 37 University of California, Riverside, CA 92521, USA
 - 38 INFN-Sezione di Roma and University of Rome, "La Sapienza", I-00185 Rome, Italy
 - 39 University and INFN, Salerno, I-84100 Salerno, Italy
 - 40 University of California, San Diego, CA 92093, USA
 - 41 Bulgarian Academy of Sciences, Central Lab. of Mechatronics and Instrumentation, BU-1113 Sofia, Bulgaria
 - 42 The Center for High Energy Physics, Kyungpook National University, 702-701 Taegu, Republic of Korea
 - 43 Purdue University, West Lafayette, IN 47907, USA
 - 44 Paul Scherrer Institut, PSI, CH-5232 Villigen, Switzerland
 - 45 DESY, D-15738 Zeuthen, Germany
 - 46 Eidgenössische Technische Hochschule, ETH Zürich, CH-8093 Zürich, Switzerland
 - 47 University of Hamburg, D-22761 Hamburg, Germany
 - 48 National Central University, Chung-Li, Taiwan, China
 - 49 Department of Physics, National Tsing Hua University, Taiwan, China
- [§] Supported by the German Bundesministerium für Bildung, Wissenschaft, Forschung und Technologie
[‡] Supported by the Hungarian OTKA fund under contract numbers T019181, F023259 and T037350.
[¶] Also supported by the Hungarian OTKA fund under contract number T026178.
^b Supported also by the Comisión Interministerial de Ciencia y Tecnología.
[‡] Also supported by CONICET and Universidad Nacional de La Plata, CC 67, 1900 La Plata, Argentina.
[△] Supported by the National Natural Science Foundation of China.

	$\langle\sqrt{s}\rangle$ [GeV]	$\int \mathcal{L}dt$ [pb]	ϵ_ℓ [%]	ϵ_{trig} [%]	N_D	N_B
$\mu^+\mu^-$	161	10.2	18.4 ± 0.5	99.4 ± 0.6	193	4
	172	9.7	18.9 ± 0.5	98.4 ± 0.8	223	7
	183	54.2	18.4 ± 0.3	99.7 ± 0.2	1188	15
	189	170.3	20.1 ± 0.3	99.6 ± 0.1	4025	33
	196	154.0	18.9 ± 0.3	99.7 ± 0.1	3491	36
	206	192.7	19.1 ± 0.2	99.7 ± 0.1	4576	45
$\tau^+\tau^-$	189	172.1	1.18 ± 0.04	71.8 ± 1.3	85	25
	196	220.9	1.29 ± 0.05	60.1 ± 1.6	97	31
	206	215.1	1.08 ± 0.04	58.0 ± 0.9	84	29

Table 1: Centre-of-mass energies and corresponding integrated luminosities. The selection efficiency, ϵ_ℓ , and trigger efficiency, ϵ_{trig} , are also given together with the number of observed events, N_D , and the background contribution, N_B .

	$\langle\sqrt{s}\rangle$ [GeV]	σ_{DATA} [pb] $ \cos\theta_\mu < 0.8$	σ_{QED} [pb] $ \cos\theta_\mu < 0.8$	σ_{DATA} [pb]	σ_{QED} [pb]
$\mu^+\mu^-$	161	$101.4 \pm 7.2 \pm 2.6$	115.4	$587 \pm 43 \pm 22$	668.3
	172	$119.2 \pm 7.6 \pm 3.1$	116.6	$700 \pm 46 \pm 27$	684.9
	183	$117.7 \pm 3.4 \pm 1.9$	118.3	$697 \pm 20 \pm 9$	700.7
	189	$117.1 \pm 1.8 \pm 1.8$	118.9	$697 \pm 11 \pm 9$	708.6
	196	$118.9 \pm 2.0 \pm 2.2$	120.3	$713 \pm 12 \pm 12$	717.8
	206	$122.6 \pm 1.8 \pm 1.7$	121.3	$738 \pm 11 \pm 8$	730.0
$\tau^+\tau^-$	189			$459 \pm 68 \pm 33$	442.6
	196			$454 \pm 67 \pm 42$	452.3
	206			$459 \pm 76 \pm 35$	466.0

Table 2: The cross sections of the processes $e^+e^- \rightarrow e^+e^-\mu^+\mu^-$ and $e^+e^- \rightarrow e^+e^-\tau^+\tau^-$ with their statistical and systematic uncertainties at different \sqrt{s} values compared to QED [8] expectations. The cross section for $e^+e^- \rightarrow e^+e^-\mu^+\mu^-$ for $3 \text{ GeV} < W_{\gamma\gamma} < 40 \text{ GeV}$ is given for both $|\cos\theta_\mu| < 0.8$ and for the full solid angle.

$W_{\gamma\gamma}$ [GeV]	$\sigma(\gamma\gamma \rightarrow \mu^+\mu^-)$ [nb]					
	$\sqrt{s} = 183$ GeV	189 GeV	196 GeV	206 GeV	183 – 209 GeV	QED
3 – 4	24.3 ± 9.9	28.0 ± 6.6	25.2 ± 6.4	27.7 ± 6.1	25.9 ± 4.2	26.8
4 – 5	21.5 ± 3.7	23.0 ± 2.7	25.2 ± 2.8	24.9 ± 3.0	22.6 ± 1.9	21.5
5 – 6	18.4 ± 1.9	18.6 ± 1.5	21.6 ± 1.6	19.1 ± 1.6	18.7 ± 1.1	18.6
6 – 7	14.5 ± 1.5	16.8 ± 1.3	18.8 ± 1.4	16.1 ± 1.3	15.9 ± 0.9	17.0
7 – 8	12.3 ± 1.5	15.3 ± 1.3	14.9 ± 1.4	18.5 ± 1.7	14.9 ± 1.0	15.2
8 – 10	11.5 ± 1.3	12.9 ± 1.0	12.4 ± 1.1	12.9 ± 1.1	12.4 ± 0.7	13.2
10 – 15	8.9 ± 1.0	9.3 ± 0.8	9.1 ± 0.8	8.3 ± 0.7	8.9 ± 0.5	9.6
15 – 20	6.0 ± 1.0	6.1 ± 0.7	6.2 ± 0.8	6.6 ± 0.8	6.2 ± 0.5	6.2
20 – 40	3.1 ± 0.6	3.3 ± 0.4	3.2 ± 0.5	3.6 ± 0.5	3.3 ± 0.3	3.2

Table 3: The cross section of the process $\gamma\gamma \rightarrow \mu^+\mu^-$ with its combined statistical and systematic uncertainties as a function of $W_{\gamma\gamma}$ for four different \sqrt{s} values and their average together with the QED [8] expectations.

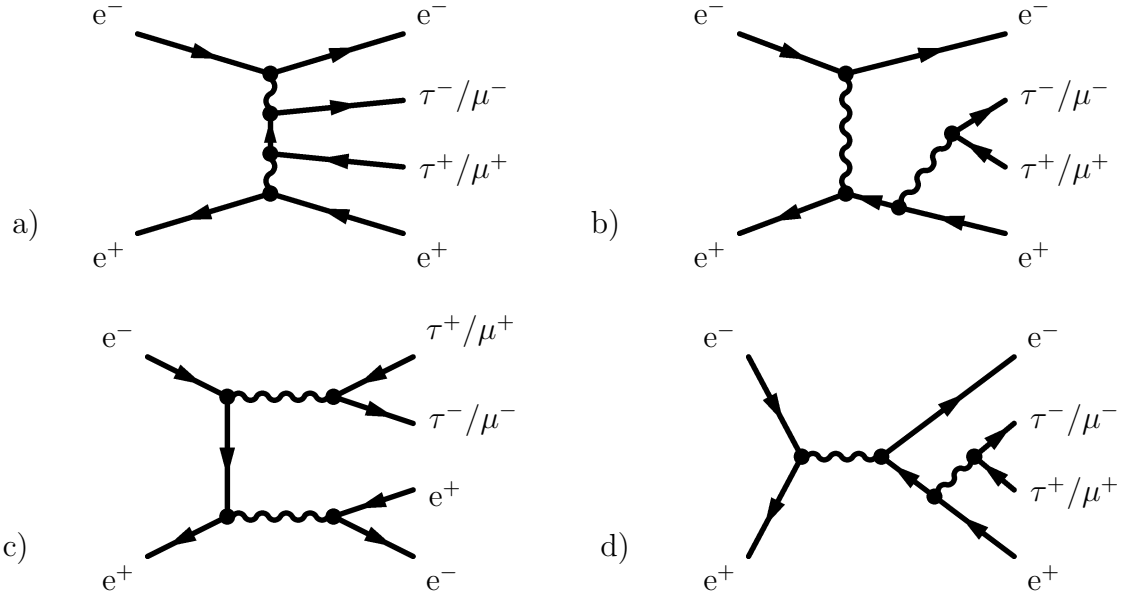


Figure 1: Feynman graphs at $\mathcal{O}(\alpha^4)$ of the processes $e^+e^- \rightarrow e^+e^-\mu^+\mu^-$ and $e^+e^- \rightarrow e^+e^-\tau^+\tau^-$: a) multiperipheral, b) bremsstrahlung, c) conversion and d) annihilation.

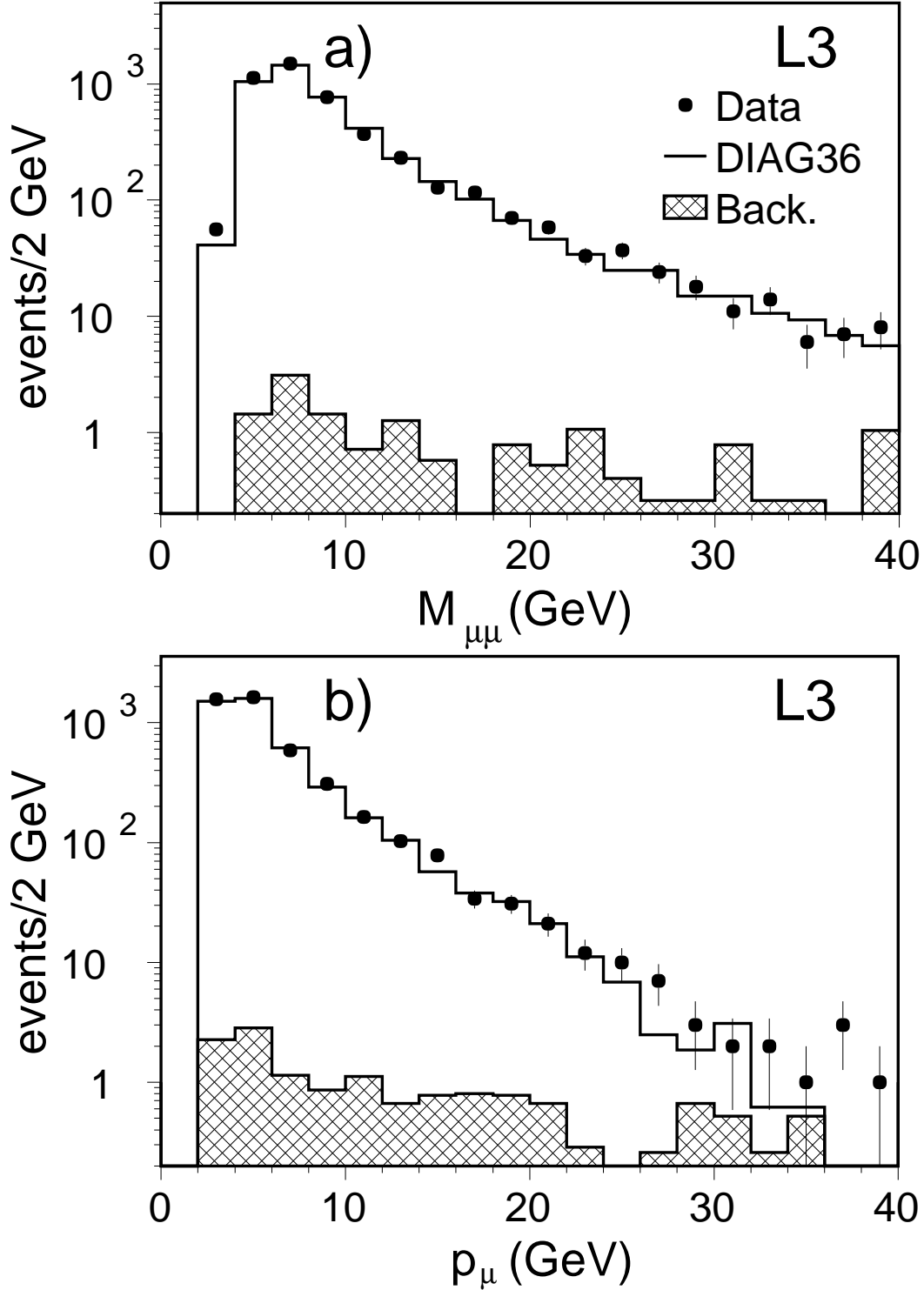


Figure 2: Distributions for selected $e^+e^- \rightarrow e^+e^-\mu^+\mu^-$ events of a) the di-muon effective mass, $M_{\mu\mu}$, and b) the momentum of the most energetic muon, p_μ . The data are compared to the sum of the DIAG36 Monte Carlo and of the expected background, normalized to the integrated luminosity.

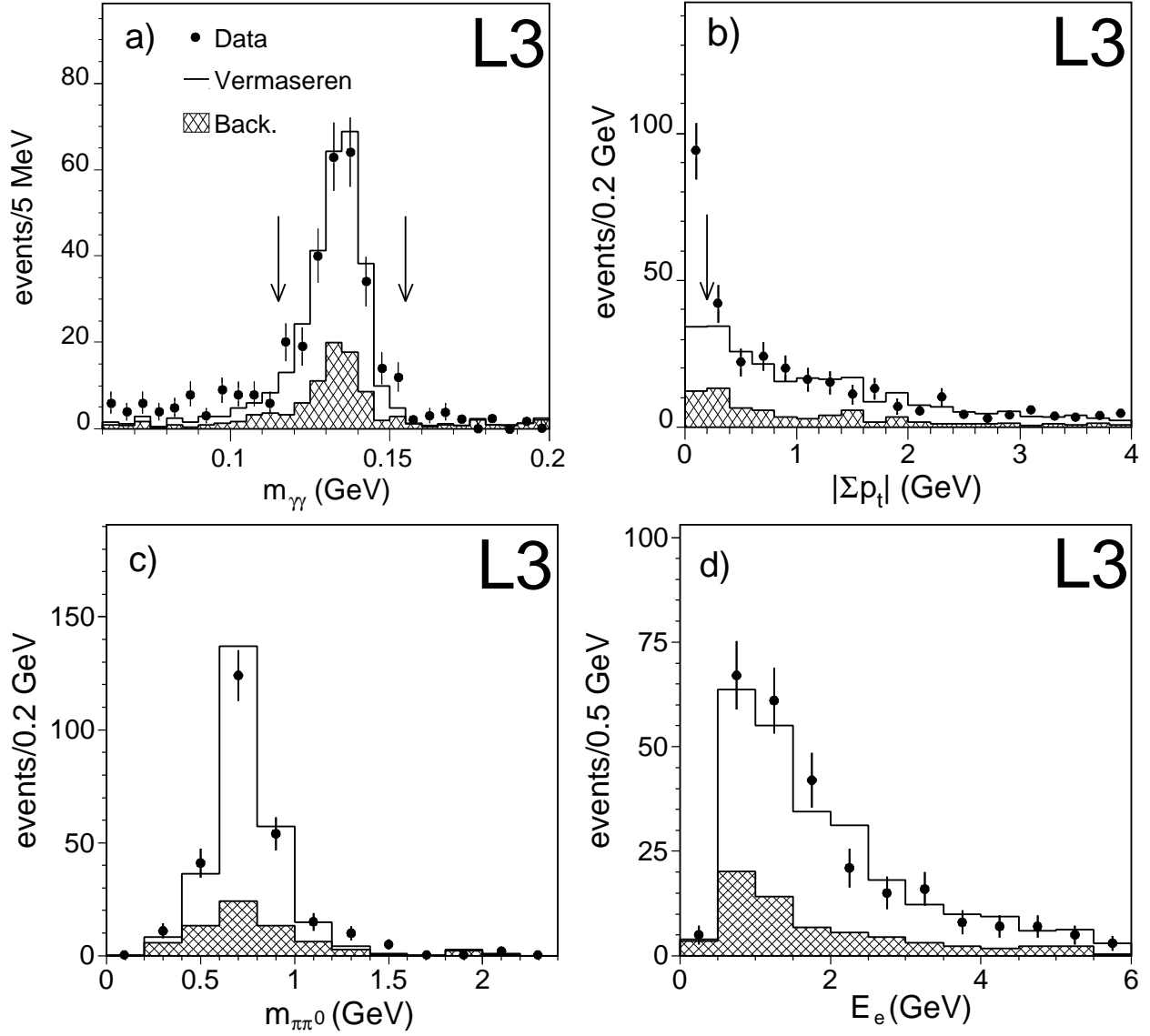


Figure 3: Distributions for $\tau \rightarrow \pi\pi\nu$ candidates of a) the effective mass of final state photons, $m_{\gamma\gamma}$, b) the sum of the transverse momenta of the charged particles, $|\sum \vec{p}_t|$, and c) the effective mass of the two pions, $m_{\pi\pi^0}$. d) Distributions of the energy of the electron for $\tau \rightarrow e\nu\nu$ candidates. The data are compared to the sum of the Vermaseren Monte Carlo $e^+e^- \rightarrow e^+e^-\tau^+\tau^-$ and of the background, normalized to the integrated luminosity. Arrows in a) and b) indicate the position of the cuts on the plotted variable, when all other selection cuts are fulfilled

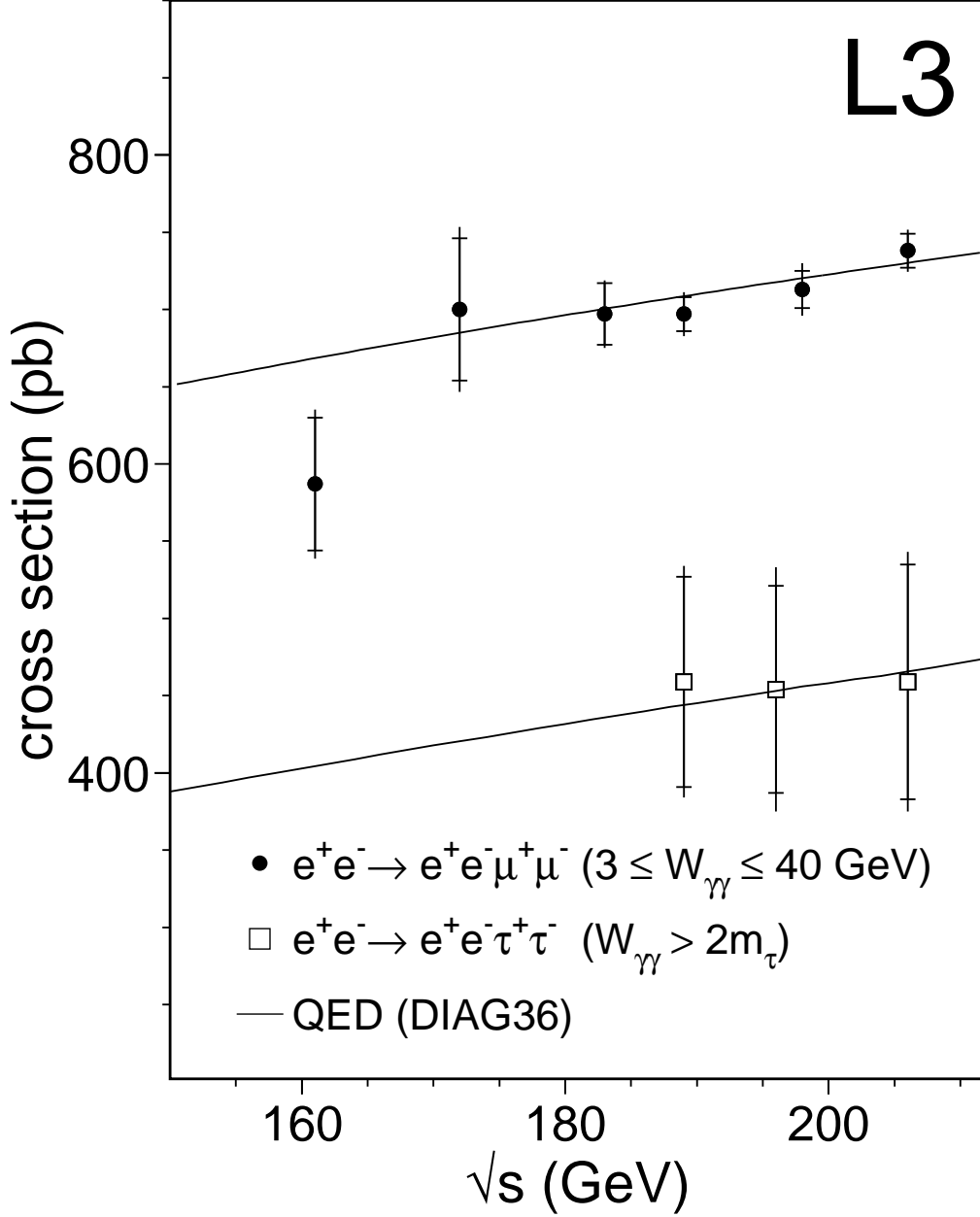


Figure 4: The cross section of the $e^+e^- \rightarrow e^+e^-\mu^+\mu^-$ process for $3 \leq W_{\gamma\gamma} \leq 40$ GeV and the total cross section of the $e^+e^- \rightarrow e^+e^-\tau^+\tau^-$ process for $W_{\gamma\gamma} > 2m_\tau$. The data are compared to the QED calculations of DIAG36. The inner parts of the error bar represent the statistical uncertainties, the outer parts the systematic uncertainties

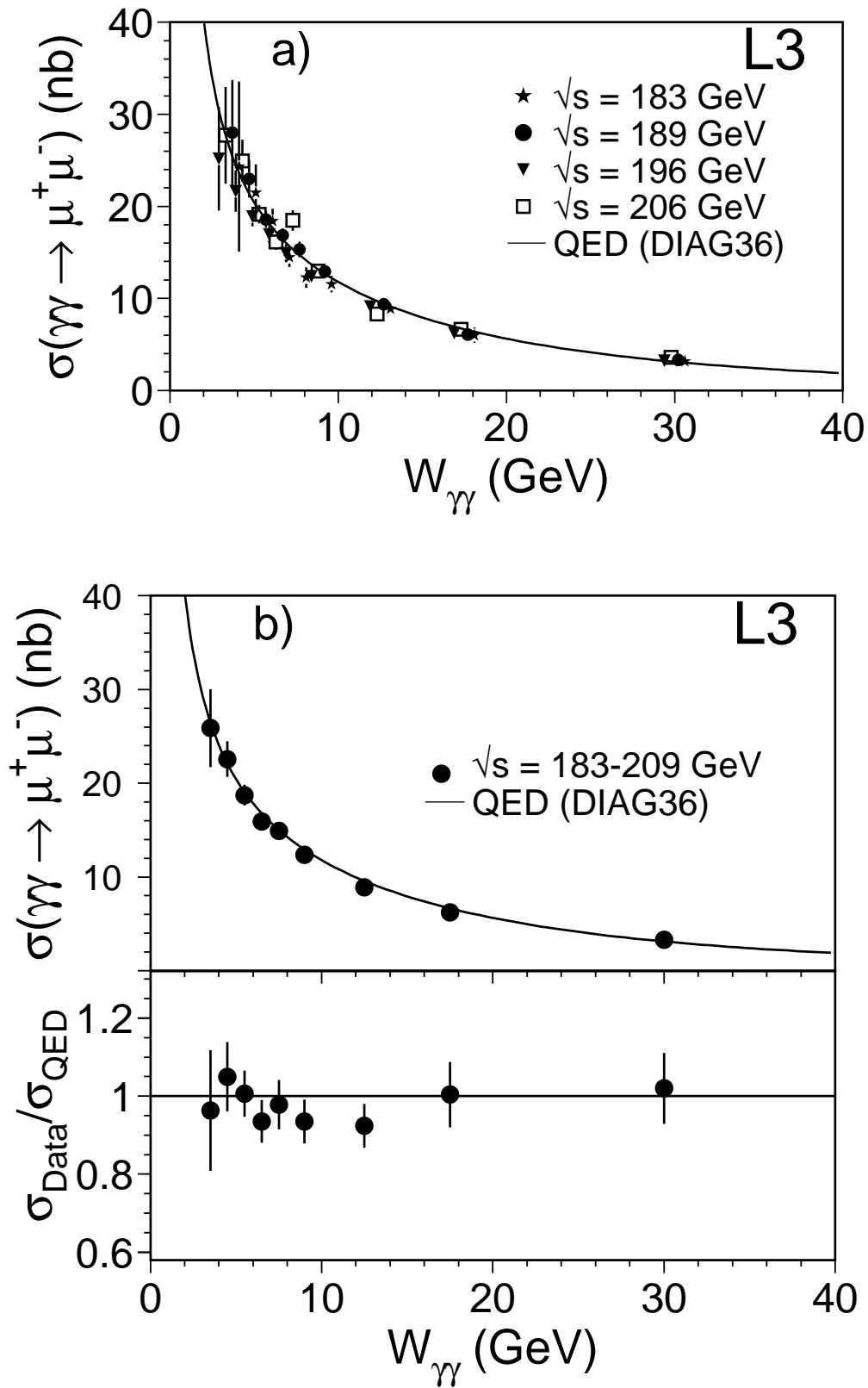


Figure 5: The cross section of the process $\gamma\gamma \rightarrow \mu^+\mu^-$ as a function of the $\gamma\gamma$ centre-of-mass energy for a) different values of \sqrt{s} and b) their combination. The data are compared to the QED calculations of DIAG36.